MULTI-ELECTRICAL EXCITATION OF A TRANSDUCER FOR ULTRASONIC IMAGING

Jian-yu Lu, Randy Kinnick, James F. Greenleaf, and Chandra M. Sehgal

Biodynamics Research Unit, Department of Physiology and Biophysics, Mayo Clinic/Foundation, Rochester, MN 55905

INTRODUCTION

Axial resolution of a transducer is a very important image quality criterion in pulse-echo imaging. It can be improved with many methods, such as using front and back matching material,[1] tapered bar shape design,[2] nonuniform distributions of piezoelectric coefficient,[3] PZT ceramic/polymer composite material,[4] as well as matched active[5,6] or passive filters.[7,8]

In this paper, a simple electrical method, multi-pulse electrical excitation (MPEE) is studied for the improvement of the axial resolution of transducers.

It is well known that a broadband transducer will usually generate a short time duration signal when it is hit by a sharp electrical unipolar pulse. Hence, high axial resolution can be obtained when such a transducer is used in pulse-echo imaging. This paper improves the performance of transducers to make them have a broader effective bandwidth.

In what follows, a theoretical model that applies linear system theory is developed to explain the operation of MPEE. We will then describe the experimental system and provide imaging and nonimaging results to support the theoretical analysis.

THEORETICAL PRELIMINARIES

Let us consider a linear transducer in the pulse-echo mode. If such a system is assumed to be linear, its transfer function is determined by,

$$H(\omega) = T(\omega) \cdot I(\omega) \cdot R(\omega), \qquad (1)$$

where $T(\omega)$ and $R(\omega)$ are the transmitting and the receiving transfer function of the transducer, and $I(\omega)$ represents the characteristics of the reflector and the acoustic pathway between the transducer and the reflector.

Double pulse excitation of a transducer can be represented as,

Acoustical Imaging, Vol. 18, Edited by H. Lee and G. Wade
Plenum Press, New York, 1991

$$S(t) = s_1(t) + ks_1(t-w), \tag{2}$$

where $s_1(t)$ and $s_1(t-w)$ represent the two exciting pulses, separated by the time interval, w, and k is the ratio of the height of the second pulse to that of the first pulse. Taking the Fourier transform of Eq. (2), one obtains

$$\mathcal{F}[S(t)] = \mathcal{F}[s_1(t)] + k\mathcal{F}[s_1(t)]\, e^{-j\omega w} \tag{3}$$

or,

$$\mathcal{F}[S(t)] = \mathcal{F}[s_1(t)]\,(1+k\, e^{-j\omega w}), \tag{4}$$

or,

$$|\mathcal{F}[S(t)]| = |\mathcal{F}[s_1(t)]| \cdot \sqrt{(1 + k^2) + 2k\cos\omega w}. \tag{5}$$

The modulus of the Fourier transform of the system output is given by

$$|\mathcal{F}[o(t)]| = |\mathcal{F}[s_1(t)]| \cdot [|H(\omega)| \cdot \sqrt{(1 + k^2) + 2k\cos\omega w}], \tag{6}$$

where $\mathcal{F}[o(t)]$ is the Fourier transform of the output of the linear system.

If $s_1(t)$ is a sharp electrical pulse, its spectrum is flat within the frequency range of interest, giving

$$|\mathcal{F}[o(t)]| \approx C \cdot [|H(\omega)| \cdot \sqrt{(1 + k^2) + 2k\cos\omega w}], \tag{7}$$

where C is a constant.

According to Eq. (7) the spectrum of the output of the transducer is modified by the weighting function. $\sqrt{(1+k^2) + 2k\cos\omega w}$. The influence of this function on transfer function is shown in Fig. 1. If w = T/2 (where T is the period corresponding to the center frequency of the system transfer function $H(\omega)$), the peak or the valley of the weighting function will overlap the center frequency portion of $H(\omega)$. The nature of the modification depends on the value of k. When k = 0, i.e., the amplitude of the second pulse is zero, the weighting function is a constant, and the output spectrum is equal to the system transfer function, which corresponds to the case of single pulse excitation. If k = 1.0, it means that the two pulses have the same amplitude, and the output spectrum exhibits a minimum at the center frequency of $H(\omega)$. If $k<0$, the weighting function has a peak at w = T/2 and the bandwidth of the spectrum of the output will be narrower than that of $H(\omega)$. For the values of $k>0$, the weighting function resembles, to some degree, the inverse of a "typical" $H(\omega)$ (see Fig. 2). It is, therefore, possible to maximize the bandwidth of the spectrum of the output by adjusting the parameter k. If $k > 1.0$, one can see from Fig. 1 that the modification of the transfer function will be weaker, therefore, the value of k should be within the range 0 to 1, in order that the best performance of the pulse echo system will be achieved. It is noted that if input signal $s_1(t)$ represents double pulses, the theory developed above can be extended to multipulse case in which the Fourier transform of $s_1(t)$ in Eq. (5), $\mathcal{F}[s_1(t)]$, is substituted by a function of the form similar to Eq. (5) itself, and the spectrum of the output of the transducer will be modified by the weighting function of higher power.

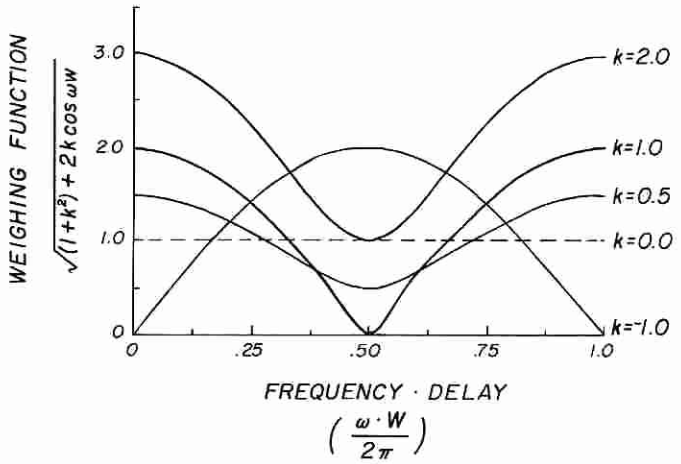

Fig. 1. Plot of the weighing function.

EXPERIMENTAL SYSTEM

Experiments were conducted with air backed and commercial (Panametric) PZT transducers. The latter was provided with matched back and front layers. The diameters for these two transducers were 17.0 mm and 12.7 mm, respectively.

The block diagram of the experimental setup is shown in Figure 3(a). Sharp electrical pulses with desired amplitudes and time delay were generated by the Polynomial Waveform Synthesizer (Data 2020). The pulses then were amplified by an ENI rf power amplifier (Model 350P and Model A300-40P) and used to excite the transducer through an impedance matching circuit.

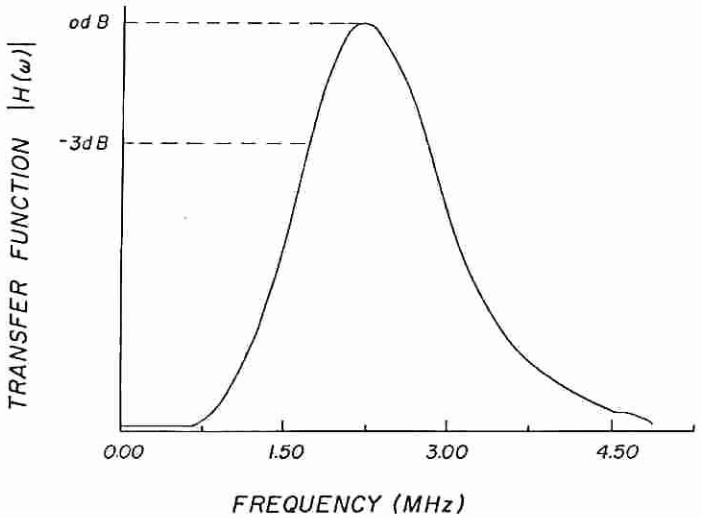

Fig. 2. "Typical" transfer function H(ω) of a commercial PZT transducer.

The reflected signal was received through T/R switch, amplified and digitized at the sampling rate of 50 MHz by a Universal Waveform Analyzer (Data 6000, Model 620). The digital data were transferred via an IEEE-488 interface to a personal computer where it was analyzed by a Scientific System (ASYST 2.0) software. The whole system was synchronized to the 1 KHz pulse sequence generated by the EXACT AM/FM Function generator (Model 7260).

Figure 3(b) shows the water tank and the scanning system. The transducers were scanned along a horizontal axis by a stepping motor. At each position, the transducer was excited and the reflected signal was digitized after a fixed time delay. On completion of the scan, the backscatter data were used to construct B-scan images. To avoid artifacts due to multiple reflection the inside walls of the water tank were lined with absorbing material. In the next section are described results of two experiments: 1) when the object in Fig. 2(b) is a simple reflector and the transducer is at a fixed position, and 2) when the reflector is a wedge phantom.

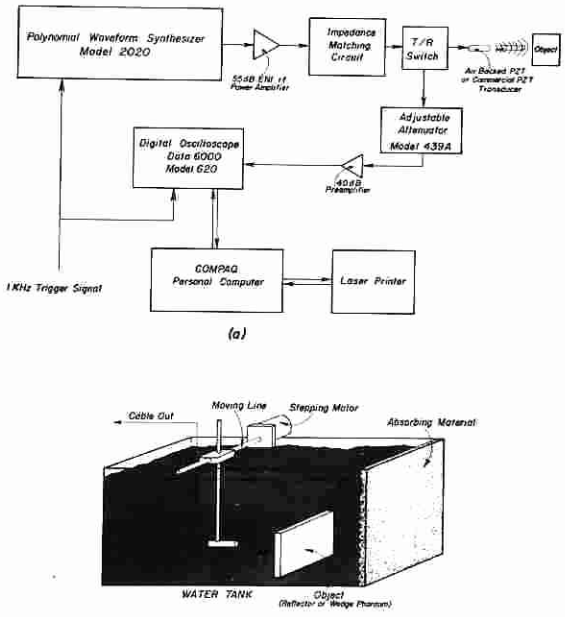

Fig. 3. Diagram of the experimental system: (a) block diagram, (b) water tank and scanning system.

RESULTS

Bandwidth Measurements

Figures 3 and 4 show the experimental results of the double pulse excitation for an air backed and the commercial PZT transducers, respectively. The center frequencies of the transducers are 2.65 MHz and 2.25 MHz, and the corresponding

half periods are 187 ns and 222 ns, respectively. The data were collected by reflecting sound energy from a flat reflector. These figures show the variation of the 3 dB bandwidth of the output signals as a function of w and k.

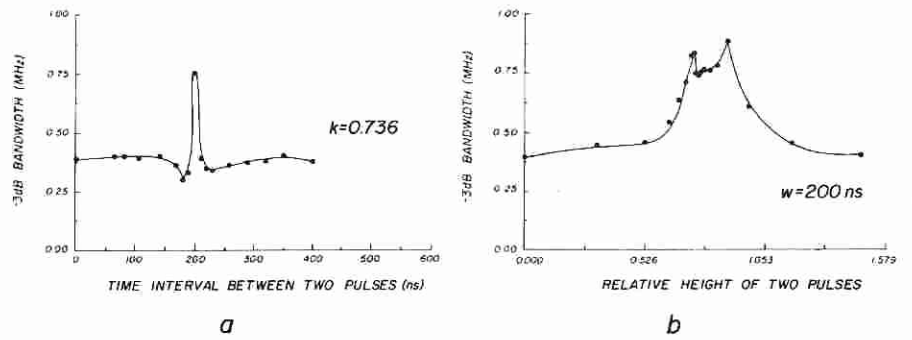

Fig. 4. Bandwidth (B) changes with w and k for the air backed PZT transducer. (a) B-w curve and (b) B-k curve.

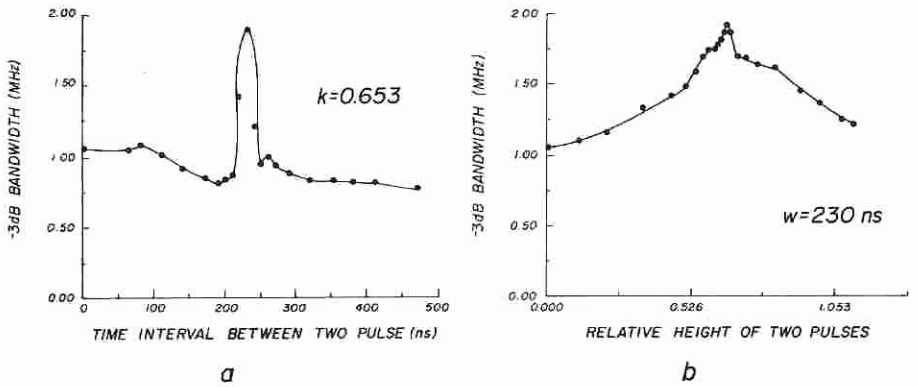

Fig. 5. Bandwidth (B) changes with w and k for the commercial PZT transducer. (a) B-w curve and (b) B-k curve.

From Figs. 4 and 5, one observes that the broadest bandwidth of the output signal is obtained for the values of w of 200 ns and 230 ns for the air backed and the commercial PZT transducers, respectively. This is consistent with the theoretical prediction that the value of w should be around the half period corresponding to the center frequency of the system transfer function.

Imaging Evaluation of MPEE

The object used for imaging was a 150 mm long wedge phantom with an adjustable gap (see Fig. 6). The phantom consisted of two plexiglas plates and was placed at 150 mm from the transducer. It was scanned in 32 steps, 5 mm apart. All the imaging results below were obtained at a sampling rate of 100 MHz. The image size is 1024 x 32 (1024 points in longitudinal axis (time axis) and 32 points in scanning axis).

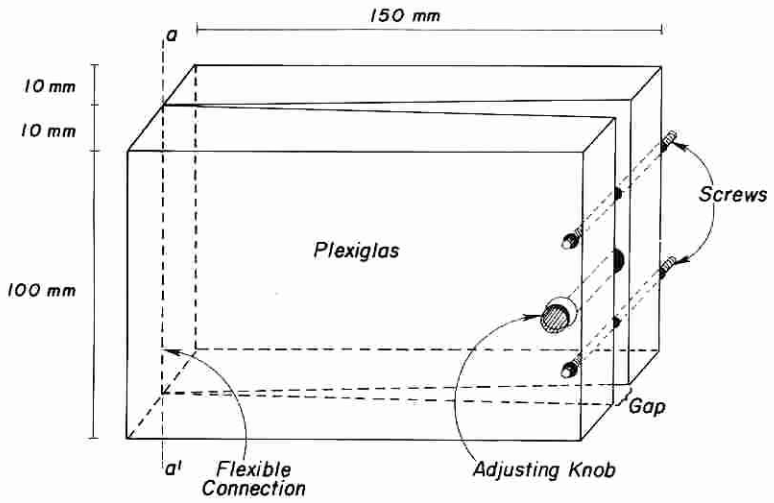

Fig. 6. Wedge phantom used in our imaging experiment.

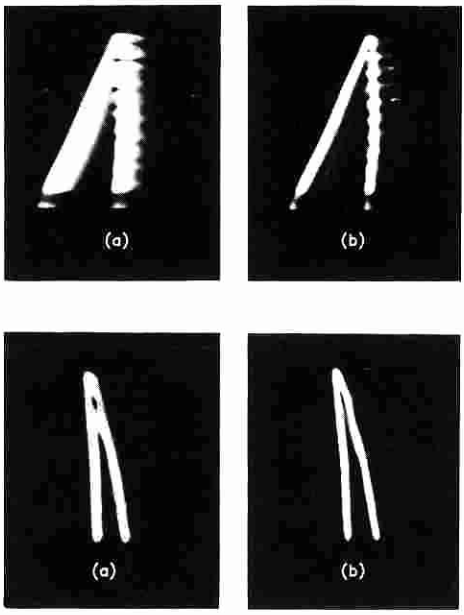

Fig. 7. Photographic displays of the images of the wedge phantom. (a) and (b) correspond to the images obtained by the single and double pulse excitation, respectively, and the images in the first row (gap = 3.30 mm) and the second row (gap 1.27 mm) are produced by the air backed and the commercial PZT transducers, respectively.

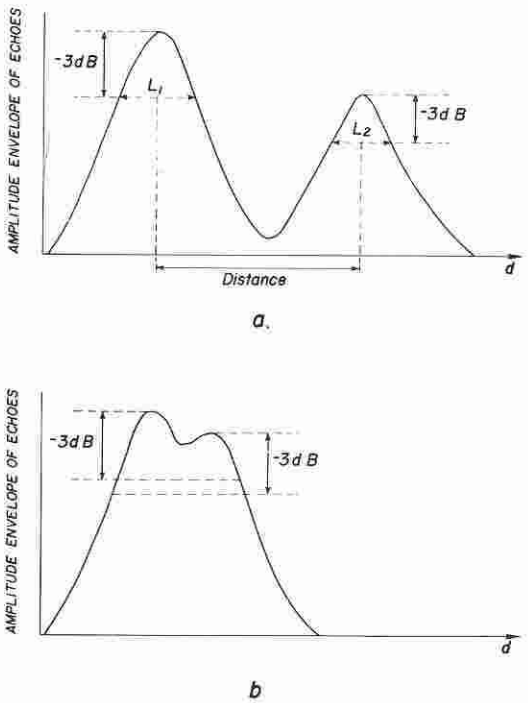

Fig. 8. Determination of distances from echoes. (a) distance is measurable, (b) distance is not measurable. The difference between (a) and (b) is the presence or absence of a valley between the -3 dB levels of the two peaks.

Figure 7 is the photographic display of the pulse-echo image of the wedge phantom. The first and second rows of the images in Fig. 7 were constructed by the air backed and the commercial PZT transducers, respectively, and the corresponding gaps of the wedge phantom used were 3.30 mm and 1.27, respectively. It is seen from these images that the MPEE improves the axial resolution significantly.

Figure 8 shows the method for the distances measured from the images. The distances were determined by first converting the output signals of the transducer into analytic envelope signals,[9] then measuring the distances between the centers of the -3 dB widths of two echoes which correspond to the reflections from two inner surfaces of the wedge phantom (see Fig. 8(a)). If the -3 dB width of the echo was not measurable, the distances were simply set to zero (see Fig. 8(b)).

Figure 9 is the comparison of the real distances of the inner walls of the wedge phantom and the distances measured from the images. If the resolution of the images in Fig. 7 is defined as the minimum real distances at which the measured distances are not zero, one can observe from Fig. 9(a) that the axial resolutions of the air backed PZT transducer are 0.99 mm and 0.44 mm with the single and double pulse excitation, respectively. Figure 9(b) shows that the axial resolutions of the commercial PZT transducer are 0.42 mm and 0.17 mm with the single and double pulse excitation, respectively.

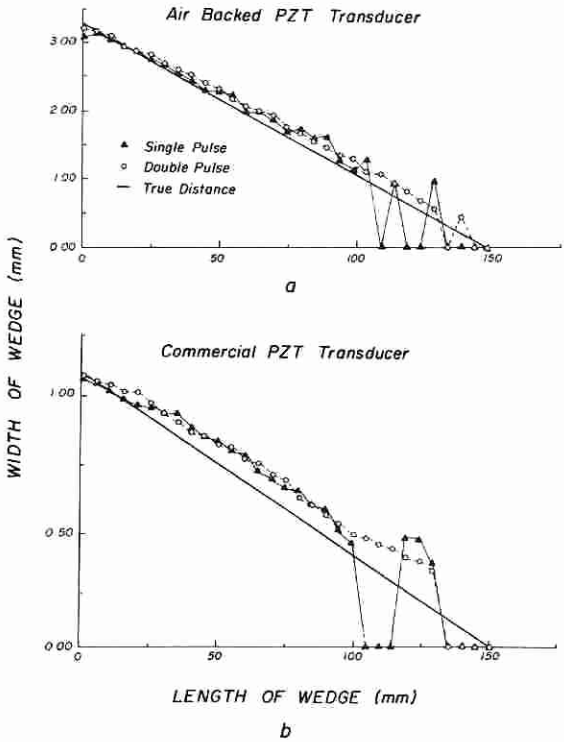

Fig. 9. Comparison of the real distances and the distances measured from the images. (a) Results of the air backed PZT transducer, (b) results of the commercial PZT transducer. Δ - single pulse and o - double pulses.

CONCLUSION

From the experimental results, Figs. 3 and 4, one can see that the bandwidth of the echo signal is greatly increased by the MPEE with the adjustment of the time interval between the two electrical excitation pulses and the ratio of the heights of the two pulses. This broadens the bandwidth of the effective transfer functions of the transducers (see Eq. (7)) and improves greatly the axial resolution of the transducers in pulse echo imaging. The results of the imaging experiment, Figs. 7 and 9, have confirmed such improvement.

It is worth noting that the MPEE is more important to the commercial PZT transducer. This is because such transducers are usually optimized by using complex backing and front matching techniques and is difficult to be improved further by conventional methods. In addition, applying the MPEE to the commercial PZT transducer does not increase low level noise[10] caused by the long ring-down tail of some transducers (the ring-down tail of the commercial PZT transducer is negligible).

ACKNOWLEDGMENTS

The authors wish to thank Elaine Quarve for secretarial assistance and Christine Welch for graphic assistance. This work was supported in part by grant 43920 from the National Institutes of Health. We also acknowledge the support of Mr. W. Harrison at Honeywell Ceramics Center for transducer design.

REFERENCES

1. G. Kossoff, The effects of backing and matching on the performance of piezoelectric ceramic transducer, IEEE Trans. Sonics Ultrason. SU-13(1):20-31, 1966.
2. P. G. Barthe and P. J. Benkeser, A staircase model of tapered piezoelectric transducers," 1987 IEEE Ultrasonics Symposium Proceedings, pp. 697-700.
3. F. Chapeau-Blondeau and J. F. Greenleaf, A theoretical model of acousto-electric transducer with a nonuniform distribution of piezoelectric coefficient. Application to transducer optimization, J. Acoust. Soc. Am. (In Press).
4. T. R. Gururaja, W. A. Schulze, I. E. Cross, and R. E. Newnham, Piezoelectric composite materials for ultrasonic transducer applications. Part II: Evaluation of ultrasonic medical applications, IEEE Trans. Sonics Ultrason. SU-32:499-513, 1985.
5. B. Mandersson and G. Salomonsson, Weighted least-squares pulse-shaping filters with application to ultrasonic signals, IEEE Trans. Ultrason. Ferroelect. Frequency Control 36(1):109-113, 1989.
6. G. Hayward and J. E. Lewis, A theoretical approach for inverse filter design in ultrasonic applications, IEEE Trans. Ultrason. Ferroelect. Frequency Control 36(3):356-364, 1989.
7. G. A. Hjellen, J. Andersen, and R. A. Sigelmann, Computer-aided design of ultrasonic transducer broadband matching networks, IEEE Trans. Sonics Ultrason. SU-21:302-305, 1974.
8. A. Yamada, On-line deconvolution for the high resolution ultrasonic pulse-echo measurement with narrow-band transducer, 1987 IEEE Ultrasonics Symposium Proceedings, pp. 1027-1030, 1987.
9. A. V. Oppenheim and R. W. Schafer, in: *Digital Signal Processing*. Prentice-Hall, Inc., Englewood Cliffs, New Jersey, Chapter 7, 1975.
10. D. H. Howry, Techniques used in ultrasonic visualization of soft tissue structures of the body, IRE Convention Becoko 3:75-88, June 9, 1955.